Nicola Basso,[1] Emanuele Soricelli,[1] Lidia Castagneto-Gissey,[1] Giovanni Casella,[1] Davide Albanese,[2] Francesca Fava,[3] Claudio Donati,[2] Kieran Tuohy,[3] Giulia Angelini,[4] Federica La Neve,[4] Anna Severino,[4] Virginia Kamvissi-Lorenz,[5,6] Andrea L. Birkenfeld,[5,6] Stefan Bornstein,[5,6] Melania Manco,[7] and Geltrude Mingrone[6,8]

Insulin Resistance, Microbiota, and Fat Distribution Changes by a New Model of Vertical Sleeve Gastrectomy in Obese Rats

Diabetes 2016;65:2990–3001 | DOI: 10.2337/db16-0039

OBESITY STUDIES

Metabolic surgery improves insulin resistance and type 2 diabetes possibly because of weight loss. We performed a novel sleeve gastrectomy in rats that resects ∼80% of the glandular portion, leaving the forestomach almost intact (glandular gastrectomy [GG]) and compared subsequent metabolic remodeling with a sham operation. GG did not affect body weight, at least after 10 weeks; improved hepatic and peripheral insulin sensitivity likely through increased Akt, glycogen synthase kinase 3, and AMPK phosphorylation; and reduced ectopic fat deposition and hepatic glycogen overaccumulation. Body adipose tissue was redistributed, with reduction of intraabdominal fat. We found a reduction of circulating ghrelin levels, increased GLP-1 plasma concentration, and remodeling of gut microbiome diversity characterized by a lower relative abundance of *Ruminococcus* and a higher relative abundance of *Lactobacillus* and *Collinsella*. These data suggest that at least in rat, the glandular stomach plays a central role in the improvement of insulin resistance, even if obesity persists. GG provides a new model of the metabolically healthy obese phenotype.

Although lifestyle changes should be the first choice for treating the global pandemic of obesity and diabetes, long-term compliance is poor (1). Metabolic surgery is, at present, the most effective therapy for morbid obesity. In the past few years, randomized controlled trials have shown that metabolic surgery is effective in determining diabetes remission in the long term (2–5). Insulin resistance is the primary defect of type 2 diabetes and plays a central role in its pathogenesis, whereas β-cell failure develops only afterward (6). Of note, some types of metabolic surgery, including biliopancreatic diversion, sleeve gastrectomy (SG), and Roux-en-Y gastric bypass, result in a net amelioration of insulin resistance with subsequent reduction of insulin secretion, even if the patient remains obese (7,8). Based on clinical observations in patients who underwent SG, we formulated a gastric hypothesis for diabetes resolution with early involvement of ghrelin and GLP-1 independent of weight change or modified food intake (9).

To understand the resolution of diabetes upon metabolic surgery, a relevant problem arises from the difficulty in separating the effect of weight loss per se from that of gastrointestinal manipulations and subsequent metabolic recovery. The rat stomach possesses two distinct portions: the proximal (forestomach), nonglandular part lined by a keratinized squamous epithelium that functions as a reservoir for food and the distal (corpus), glandular part

[1]Surgical-Medical Department for Digestive Diseases, Policlinico Umberto I, University of Rome Sapienza, Rome, Italy
[2]Computational Biology, Research and Innovation Centre-Fondazione Edmund Mach, San Michele all'Adige, Trento, Italy
[3]Department of Food Quality and Nutrition, Research and Innovation Centre-Fondazione Edmund Mach, San Michele all'Adige, Trento, Italy
[4]Institute of Cardiology, Catholic University, Rome, Italy
[5]Department of Medicine III, Universitätsklinikum Carl Gustav Carus an der Technischen Universität Dresden, Dresden, Germany
[6]Diabetes and Nutritional Sciences, King's College London, London, U.K.
[7]Research Unit for Multifactorial Diseases, Scientific Directorate, Bambino Gesù Children Hospital, Rome, Italy
[8]Department of Internal Medicine, Catholic University, Rome, Italy

Corresponding author: Geltrude Mingrone, geltrude.mingrone@unicatt.it or geltrude.mingrone@kcl.ac.uk.

Received 9 January 2016 and accepted 8 July 2016.

This article contains Supplementary Data online at http://diabetes.diabetesjournals.org/lookup/suppl/doi:10.2337/db16-0039/-/DC1.

lined by a simple columnar epithelium responsible for exocrine and endocrine secretions (10). The modified SG or glandular gastrectomy (GG) devised by us resects ~80% of the glandular portion to induce hormonal effects but leaves the nonglandular portion almost intact, thereby limiting loss of gastric volume and its sequelae on body weight. In high-fat diet (HFD)–fed obese rats, the effect of GG on body fat distribution, insulin sensitivity, insulin signaling, and gut microbiota was compared with that of a gastric sham operation (SO).

RESEARCH DESIGN AND METHODS

Animals

Sixty male Wistar rats aged 10 weeks were housed individually in hanging wire cages in a controlled room at 22°C with a 12-h day/night cycle (lights on 0700–1900 h). The animals received a purified tripalmitin-based HFD ad libitum (Rieper AG, Bolzano, Italy) with an energy density of 21.10 kJ/g that supplied 59% of energy from fat and 20% from carbohydrate comprising cornstarch and sucrose (2:1 weight for weight) and containing corn oil (1.9/100 g diet) to prevent essential fatty acid deficiency. The HFD was continued for 10 weeks before and 10 weeks after the operation.

The animals randomly underwent GG or SO. Survival rates were 90% after SO and 75% after GG. All experimental procedures were approved by the Catholic University of Rome Institutional Animal Care Committee.

Interventions

The rats were anesthetized using ketamine (75 mg/kg intramuscularly) and xylazine (10 mg/kg intramuscularly). Ten milliliters of sterile 0.9% NaCl were administered subcutaneously before surgery.

Access to the peritoneal cavity was obtained by 3-cm laparotomy. About 80% of the glandular stomach was removed by resecting the organ along a line (Supplementary Fig. 1), and the nonglandular forestomach was left almost intact. The gastric remnant was closed by single-layer continuous suture using 6-0 Prolene thread (Ethicon, Somerville, NJ). The SO rats had the same anesthesia. A midline laparotomy was performed, and the stomach was exposed and gently manipulated. The abdominal cavity was kept open for the same amount of time required to perform GG. A 1-cm gastrotomy was performed and then closed as in the previous group.

Postoperative Care

At the end of the surgical procedures, all rats received sterile 0.9% NaCl 10 mL i.p. and 10 mL s.c. to maintain hydration during healing. The animals received ketoprofen 5 mg/kg as an analgesic. They were placed on a heated mat until they recovered and then were returned to their home cages. The rats were allowed to drink purified water for 12 h after surgery, and a liquid diet containing 5% glucose and 0.2% KCl was provided for the next 48 h. Thereafter, they received the HFD until 10 weeks after surgery.

Oral Glucose Tolerance Test

The oral glucose tolerance test (OGTT) was performed at kill. Animals were fasted overnight and then received a 50% D-glucose solution (1g/kg body weight) by oral gavage. Blood was collected from the tail vein for measurement of glucose and insulin concentrations at 0, 15, 30, 60, 90, and 120 min at the end of the study. At the end of the OGTT, blood was obtained by cardiac puncture and placed in tubes containing EDTA, aprotinin, and a dipeptidyl peptidase 4 (DPP-4) inhibitor and analyzed for GLP-1 and ghrelin. After centrifugation, plasma was divided into appropriate subsamples and stored at −20°C until analyses.

Histology

SO and GG rats were killed, and fresh portions of liver, muscle, and adipose tissue from each rat were cut, fixed in neutral buffered formalin (10%), and dehydrated using gradations of ethanol (70%, 80%, 90%, 95%, and 100%). Dehydration was followed by clearing the samples in two changes of xylene. The samples were then embedded in paraffin and cut with a microtome (3–4 μm). Hematoxylin and eosin staining was used. Periodic acid Schiff staining was used to evaluate glycogen storage. Photographs of stained sections were taken with an optical microscope (ZEISS Primo Star HAL/LED).

Western Blot Analysis

Muscle biopsy specimens were rinsed in PBS and homogenized in radioimmunoprecipitation assay buffer containing a cocktail of protease inhibitors. Homogenates were cleared by centrifugation (13,000 rpm) for 30 min at 4°C. Protein content was determined using Bradford Protein Assay (Bio-Rad).

Protein lysates (30 μg) were separated on 8% SDS-PAGE and transferred on polyvinylidene fluoride membrane. Membranes were probed overnight with the following antibodies: pAktSer473 (D9E), pAMPKα, and glycogen synthase kinase 3 (GSK3) α-β Ser21/9 (9331). Membranes were stripped for 30 min at 56°C and reprobed overnight with Aktpan (C67E7), AMPKα (D5A2), and GSK3α-β (D75D3), respectively. All the antibodies were from Cell Signaling. Detection and analysis were performed with the ChemiDoc XRS system with Image Lab 5.0 software (Bio-Rad). All results are expressed as a phosphoprotein/total protein ratio.

16S rRNA Gene Sequencing by Roche GS FLX+ Platform

Bacterial genomic DNA was extracted from rat fecal samples by using the FastDNA SPIN Kit for Feces (MP Biomedicals). The V3–V5 16S rRNA gene variable regions were amplified by PCR using 454 adapter-linked and bar-coded primers 338F (5′-TCCTACGGGAGGCAGCAG-3′) and 934R (5′-TGTGCGGGCCCCCGTCAATT-3′). Each PCR reaction was carried out in triplicate with 0.2 μmol/L deoxynucleotides, 0.4 μmol/L primers, 0.05 units Taq DNA Polymerase (FastStart High Fidelity PCR System; Roche, Basel, Switzerland), and 40 ng template DNA. The following thermal cycles were used: 95°C for 5 min; 30 cycles at 95°C for 30 s, 58°C for 30 s, and 72°C for 1 min; and a final elongation step at 72°C for 8 min. PCR products were analyzed by lab-on-a-chip electrophoresis (2100 Bioanalyzer; Agilent Technologies, Santa Clara, CA) and cleaned by using

the Agencourt AMPure XP system (Beckman Coulter, Brea, CA) following the manufacturer's instructions. Purified products underwent quantitative PCR (LightCycler 480; Roche) by using the KAPA Library Quantification Kit (KAPA Biosystems, Boston, MA) and pooled equimolarly in a final amplicon library. The pyrosequencing was carried out on the GS FLX+ system using XL+ chemistry (454 Life Sciences, Roche) following the manufacturer's recommendations.

DNA pyrosequencing resulted in a total of 1,088,841 partial 16S rRNA gene reads with a mean of 35,123 sequences per sample. Average sequence lengths were 671 nucleotides with an average Phred quality score of 31. Raw 454 files were demultiplexed by using Roche sff file software and are available at the European Nucleotide Archive (www.ebi.ac.uk) under the accession study PRJEB11901. Sample accessions and metadata are available in Supplementary Table 1. Reads were preprocessed by using the MICrobial Community Analysis pipeline version 0.1 (http://micca.org). Forward and reverse primer trimming and quality filtering were performed using micca-preproc (parameters -fTCCTACGGGAGGCAGCAG -rTGTGCGGGCCCCCGTCAATT-O 16 -q 20 -l 300), truncating reads <300 nucleotides. De novo sequence clustering, chimera filtering, and taxonomy assignment were performed by micca-otu-denovo (parameters -s 0.97 -d -l 200 -c). Operational taxonomic units were assigned by clustering the sequences with a threshold of 97% pairwise identity, and their representative sequences were classified using Remote Desktop Protocol software version 2.8. Template-guided multiple sequence alignment was performed using PyNAST version 0.1 against the multiple alignment of the Greengenes database (release 13_05) filtered at 97% similarity. Finally, a phylogenetic tree was inferred using FastTree and micca-phylogeny (parameters: -a template-template-min-perc 75). Sampling heterogeneity was reduced by rarefaction (12,562 sequences/sample). An α-diversity (within-sample richness) and a β-diversity (between-sample dissimilarity) estimate were computed using the phyloseq R package. Permutational ANOVA tests were performed by using the adonis function of the vegan R package with 999 permutations. The random forest model was computed using the supervised_learning.py script of QIIME version 1.8.0 (10.1038/nmeth.f.303), with 1,000 trees and 10-fold cross-validation.

Analytical Methods

Plasma glucose levels were analyzed by the glucose oxidase method (Glucose Analyzer II; Beckman Coulter, Fullerton, CA). The plasma concentrations of cholesterol and triacylglycerol (TAG) were measured using spectrophotometric methods. Serum insulin was measured by a rat insulin ultrasensitive ELISA (BioVendor, Kassel, Germany), with a sensitivity of 0.025 ng/mL and an intra- and interassay precision of 10%. Plasma GLP-$1_{7–36}$ and active ghrelin were measured by rodent/rat-specific ELISAs (Millipore, St. Charles, MO). Sensitivity was 5.2 pg/mL, intraassay <11%, interassay <19%, and accuracy 83% for GLP-$1_{7–36}$. The intraassay was 1–6%, the interassay 1–5%, and the accuracy 94–105% for ghrelin. Total plasma bile acids (BAs) were determined with a BA assay kit (Trinity Biotech, Jamestown, NY). Plasma lipopolysaccharide (LPS) levels were determined using a Limulus Amebocyte Lysate Kit (QCL-1000; Lonza, Walkersville, MD).

Statistical Analysis

Data are expressed as mean ± SEM. The HOMA for insulin resistance (HOMA-IR) index (11) was calculated as fasting blood glucose (mg/dL) × fasting plasma insulin (μU/mL)/405. The factor 405 accounts for measurement units.

The incremental areas under the curve (AUCs) were computed by using the trapezoidal rule. Insulin sensitivity after the OGTT was measured as the glucose/insulin AUC ratio. Glucose and insulin AUC data intragroup variations were assessed by Wilcoxon test, whereas intergroup differences were assessed by Mann-Whitney *U* test due to lack of normal distribution by Shapiro-Wilk test.

Differences were considered significant at $P < 0.05$. Spearman correlation analysis was performed to detect the correlations among variables.

RESULTS

All animals lost weight in the week following surgery with ~10% weight loss in the SO and 15% in the GG group. Rats in the GG group recovered more slowly but from the third week after surgery, their weight was not statistically different from that of SO animals (Supplementary Fig. 2*A*). Food intake also did not differ between the groups from week 3 postsurgery (Supplementary Fig. 2*B*).

At 10 weeks after the operation, mesenteric and retroperitoneal fat content was higher in the SO than in the GG group (9.67 ± 1.26 vs. 8.11 ± 1.22 g [$P < 0.01$] and 8.75 ± 1.16 vs. 7.30 ± 0.95 g [$P < 0.01$], respectively). In contrast, subcutaneous fat was more represented in GG than in SO rats (2.64 ± 0.65 vs. 4.10 ± 0.78 g, $P < 0.0001$).

Insulin Sensitivity

The data in Table 1 and Figs. 1–6 refer to the end of the study. Insulin sensitivity was significantly improved in GG compared with SO rats as demonstrated both by HOMA-IR values, which were reduced by ~50%, and by the $AUC_{glucose}/AUC_{insulin}$ ratio, which was ~55% lower in GG than in SO animals (Table 1). The time courses of blood glucose and plasma insulin concentrations after the OGTT are reported in Fig. 1*A* and *B*, respectively. Despite that the glycemic curve was significantly lower after GG than after SO, blood glucose levels did not return to the baseline. Both cholesterol and TAG levels dropped in GG rats (Table 1).

Active plasma ghrelin levels (Table 1) in GG rats (2.24 ± 4.04 vs. 48.32 ± 5.38 fmol/mL), were significantly reduced ($P < 0.0001$) with respect to the SO group. Plasma levels of GLP-1 were significantly higher ($P < 0.0001$) in GG rats (5.15 ± 1.52 pmol/mL) compared with SO rats (3.01 ± 0.84 pmol/mL) (Table 1). We cannot exclude a more rapid gastric emptying after GG, which

Table 1—Weight and metabolic parameters in SO and GG rats

	GG	SO	*P* value
Weight (g)	299.83 ± 47.21	296.15 ± 55.56	0.953
Fasting plasma glucose (mg/dL)	138.76 ± 21.39	166.47 ± 28.18	0.001
Fasting plasma insulin (ng/mL)	1.27 ± 0.25	2.42 ± 0.67	<0.0001
HOMA-IR	14.93 ± 3.20	23.72 ± 7.10	<0.0001
Glucose AUC	11,753.57 ± 8,024.38	17,210.16 ± 5,554.65	0.029
Insulin AUC	138.24 ± 55.66	254.53 ± 114.01	0.001
$AUC_{glucose}/AUC_{insulin}$	64.53 ± 62.90	143.32 ± 70.70	0.001
Cholesterol (mg/dL)	122.33 ± 9.55	167.81 ± 25.21	<0.0001
TAG (mg/dL)	133.28 ± 10.23	189.85 ± 21.40	<0.0001
Ghrelin (fmol/mL)	4.20 ± 11.75	48.69 ± 5.79	<0.0001
GLP-1 (pmol/mL)	5.15 ± 1.57	2.93 ± 0.93	<0.0001
LPS (EU/mL)	4.65 ± 0.87	7.84 ± 0.98	<0.0001
BAs (μmol/L)	22.96 ± 3.79	14.17 ± 2.76	<0.0001

Data are mean ± SD. Blood samples were taken at kill. Significance was computed by Wilcoxon signed rank test. EU, endotoxin unit.

could have stimulated GLP-1 secretion. LPS levels were almost halved, whereas BAs were nearly doubled in GG compared with SO rats (Table 1).

Table 2 shows the Spearman correlation coefficients between relevant metabolic and microbial measures. In a multiple regression analysis (R^2 = 0.84, $P < 0.0001$) with HOMA-IR as the dependent variable and ghrelin, GLP-1, BAs, TAG, and mesenteric and retroperitoneal fat as independent variables, the significant predictors were ghrelin (β = 0.26, P = 0.034), GLP-1 (β = −0.32, P = 0.019),

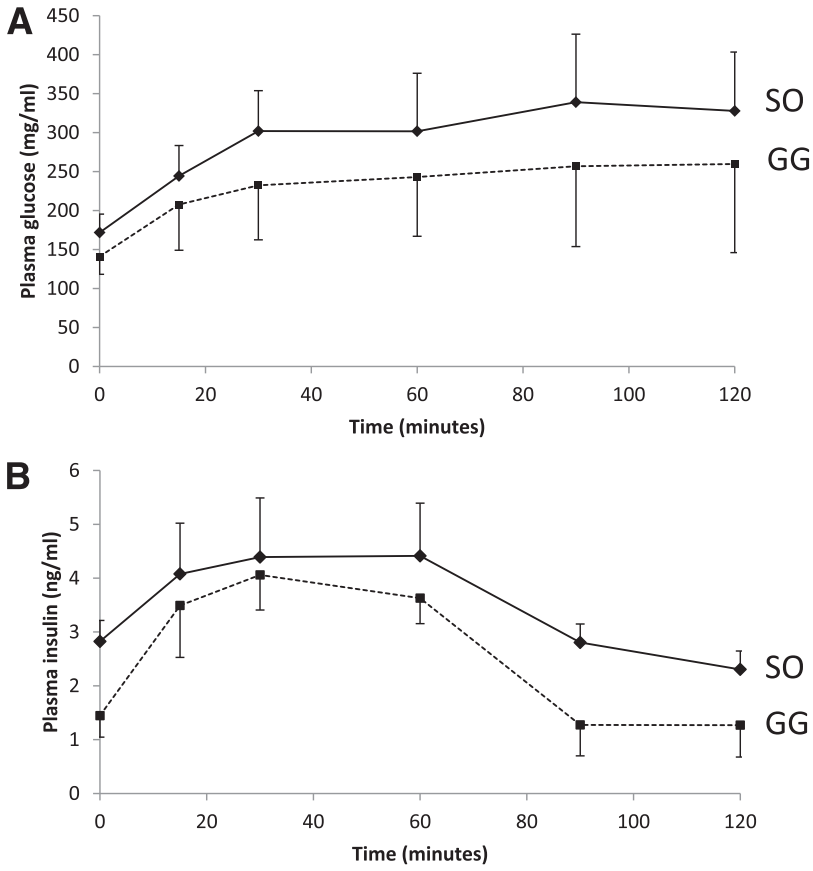

Figure 1—Time courses of plasma glucose (*A*) and plasma insulin (*B*) in SO and GG rats. Both plasma glucose and insulin concentrations were reduced in GG compared with SO rats. The OGTT was performed the day of kill.

Table 2—Spearman correlation coefficients between relevant metabolic and microbial measures within the GG rats (n = 18)

	Spearman correlation coefficients													
Variable	GRL	GLP-1	Cholesterol	TAG	HOMA-IR	Weight	Mesenteric adipose tissue	Retroperitoneal adipose tissue	Subcutaneous adipose tissue	LPS	BA	*Lacto-bacillus*	*Collinsella*	*Ruminococcus*
GRL	1.00	−0.52*	0.01	0.32	0.70*	0.09	0.42	0.31	−0.02	0.18	−0.39	0.22	−0.49*	0.20
GLP-1	−0.52*	1.00	−0.07	−0.36	−0.64*	−0.31	−0.36	−0.33	−0.10	−0.08	0.21	−0.14	0.09	0.08
Cholesterol	0.01	−0.07	1.00	0.53*	0.45	0.61*	0.65*	0.69*	0.79*	0.64*	−0.55*	0.20	0.02	−0.55*
TAG	0.32	−0.36	0.53*	1.00	0.64*	0.80*	0.52*	0.54*	0.56*	0.50*	−0.25	0.29	−0.16	−0.33
HOMA-IR	0.70*	−0.64*	0.45	0.64*	1.00	0.45	0.57*	0.50*	0.40	0.42	−0.62*	0.17	−0.30	−0.19
Weight	0.09	−0.31	0.61*	0.80*	0.45	1.00	0.55*	0.59*	0.53*	0.46	−0.08	0.14	0.05	−0.45
Mesenteric adipose tissue	0.42	−0.36	0.65*	0.52*	0.57*	0.55*	1.00	0.97*	0.61*	0.47*	−0.54*	0.36	0.05	−0.52*
Retroperitoneal adipose tissue	0.31	−0.33	0.69*	0.54*	0.50*	0.59*	0.97*	1.00	0.67*	0.52*	−0.54*	0.42	0.08	−0.57*
Subcutaneous adipose tissue	−0.02	−0.10	0.79*	0.56*	0.40	0.53*	0.61*	0.67*	1.00	0.43	−0.38	0.26	0.19	−0.69*
LPS	0.18	−0.08	0.64*	0.50*	0.42	0.46	0.47*	0.52*	0.43	1.00	−0.65*	0.16	−0.34	−0.08
BA	−0.39	0.21	−0.55*	−0.25	−0.62*	−0.08	−0.54*	−0.54*	−0.38	−0.65*	1.00	−0.17	0.20	0.13
Lactobacillus	0.22	−0.14	0.20	0.29	0.17	0.14	0.36	0.42	0.26	0.16	−0.17	1.00	0.03	−0.21
Collinsella	−0.49*	0.09	0.02	−0.16	−0.30	0.05	0.05	0.08	0.19	−0.34	0.20	0.03	1.00	−0.69*
Ruminococcus	0.20	0.08	−0.55*	−0.33	−0.19	−0.45	−0.52*	−0.57*	−0.69*	−0.08	0.13	−0.21	−0.69*	1.00

GRL, ghrelin. *$P < 0.05$.

BA (β = −0.26, *P* = 0.040), and TAG (β = 0.49, *P* = 0.002) levels.

Ectopic Fat Deposition and Hepatic Glycogen

Because fat deposition in muscle and liver is associated with insulin resistance, the histological effects of both surgical procedures in these sites were evaluated. Skeletal muscle fat infiltration was present in SO but not in GG rats (Fig. 2*A* and *B*). All SO animals showed moderate to marked hepatic steatosis and some ballooning degeneration (Fig. 2*C*). GG rats showed normal liver architecture (Fig. 2*D*). Furthermore, SO rats exhibited higher glycogen liver storage than GG rats (Fig. 2*E* and *F*). Finally, an increase in both interstitial cellular infiltration and fibrosis was observed in the visceral adipose tissue of SO rats compared with GG rats (Fig. 2*G* and *H*).

Western Blots

When compared with SO rats, GG rats exhibited increased phosphorylation of Akt on Ser473 in muscle (21.5 ± 8.2 vs. 74.03 ± 11.8%, *P* = 0.006) (Fig. 3*A*, left) and in liver (8.7 ± 0.8 vs. 13.9 ± 1.7%, *P* = 0.03) (Fig. 3*B*, left). No significant difference of Akt phosphorylation in the subcutaneous adipose tissue (16.1 ± 3.4 vs. 9.4 ± 3.4%) (Fig. 3*C*, left) and GSK3β phosphorylation in both muscle (7.4 ± 0.5 vs. 9.4 ± 0.2%, data not shown) and adipose tissue (38.7 ± 11.2 vs. 12.8 ± 3.3%) (Fig. 3*C*, right) between SO and GG rats was observed. The liver showed increased GSK3β phosphorylation in GG rats compared with SO rats (4.6 ± 1.3 vs. 10.5 ± 2.0%, *P* = 0.049) (Fig. 3*B*, right). GSK3α isoform phosphorylation (Ser21) in the muscle showed no significant differences between SO and GG rats (5.3 ± 1.0 vs. 6.5 ± 2.2%), whereas it was not detectable in the liver and adipose tissue. The muscle phosphorylated AMPKα (Tyr172) form was 53% higher in GG than in SO rats (1.9 ± 0.18 vs. 2.9 ± 0.2%, *P* = 0.007) (Fig. 3*A*, right).

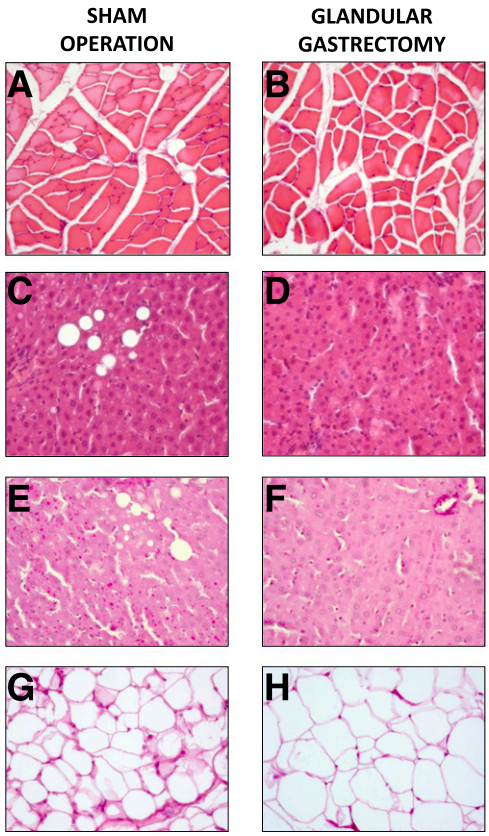

Figure 2—Representative hematoxylin and eosin–stained muscle sections from SO and GG rats fed an HFD. SO rats exhibited predominantly steatosis in muscle (*A*) and liver (*C*) sections. GG rats showed no steatosis in muscle (*B*) and liver (*D*) sections. Representative periodic acid Schiff–stained sections of liver from SO and GG rats fed an HFD. SO rats exhibited a higher glycogen storage in liver sections (*E*). GG rats showed a decrease in glycogen deposition in liver sections (*F*). SO rats showed abundant interstitial cellular infiltration (possibly macrophages) of the retroperitoneal adipose tissue with pronounced fibrosis (*G*); these features were absent in GG rats (*H*). Original magnification ×20.

Gut Microbiota

GG wrought significant changes in microbiome structure, with GG animals showing significantly higher taxa richness (α-diversity) as calculated by the Shannon index (*P* = 0.0064, Wilcoxon rank sum test, false discovery rate corrected) (Fig. 4*A*). GG and SO rats were significantly different in terms of β-diversity based on unweighted UniFrac (Fig. 4*B*), weighted UniFrac, and Bray-Curtis between-sample dissimilarity measures (*P* = 0.002, 0.034, and 0.002, respectively, by permutational ANOVA test).

Differences in the relative abundance of bacteria within the gut microbiota of GG and SO rats are shown in Fig. 5 at various taxonomic levels (phylum to genus). No statistically significant differences were observed between the groups at the phylum level. At the class level, γ-Proteobacteria (*P* = 0.020), Actinobacteria (*P* = 0.034), Bacilli ($P = 8.0 \times 10^{-5}$), and Erysipelotrichia (*P* = 0.016) were all significantly enriched in the GG group compared with the SO group, whereas the Clostridia were enriched in the SO group (*P* = 0.031). At the order level, Aeromonadales (*P* = 0.04), Actinomycetales (*P* = 0.03), Coriobacteriales (*P* = 0.04), Lactobacillales (*P* < 0.0001), Clostridiales (*P* = 0.03), and Erysipelotrichales (*P* = 0.02) differed between groups. According to the Wilcoxon rank sum test, significant differences occurred between GG and SO rats at the genus level, with GG animals harboring higher relative abundance of *Lactobacillus* (*P* = 0.0003) and *Collinsella* (*P* = 0.0095), whereas SO animals had higher *Ruminococcus* (*P* = 0.0095).

To define bacteria characteristic of the GG or SO groups at the order and genus taxonomic levels, we performed a random forest model in a 10-fold cross-validation scheme, obtaining an estimated test error of 13.3 ± 18.5% (order level abundances) and 12.5 ± 22.65% (genus level abundances). The top-ranked orders and genera (mean decrease in classification accuracy >0.1%) identified by random forest models are shown in Fig. 6 in decreasing order of their discriminatory importance. Lactobacilli were the main drivers of the difference between groups at both taxonomic levels.

DISCUSSION

We describe the results of a novel experimental model of metabolic surgery, the GG, which is associated with *1*) a

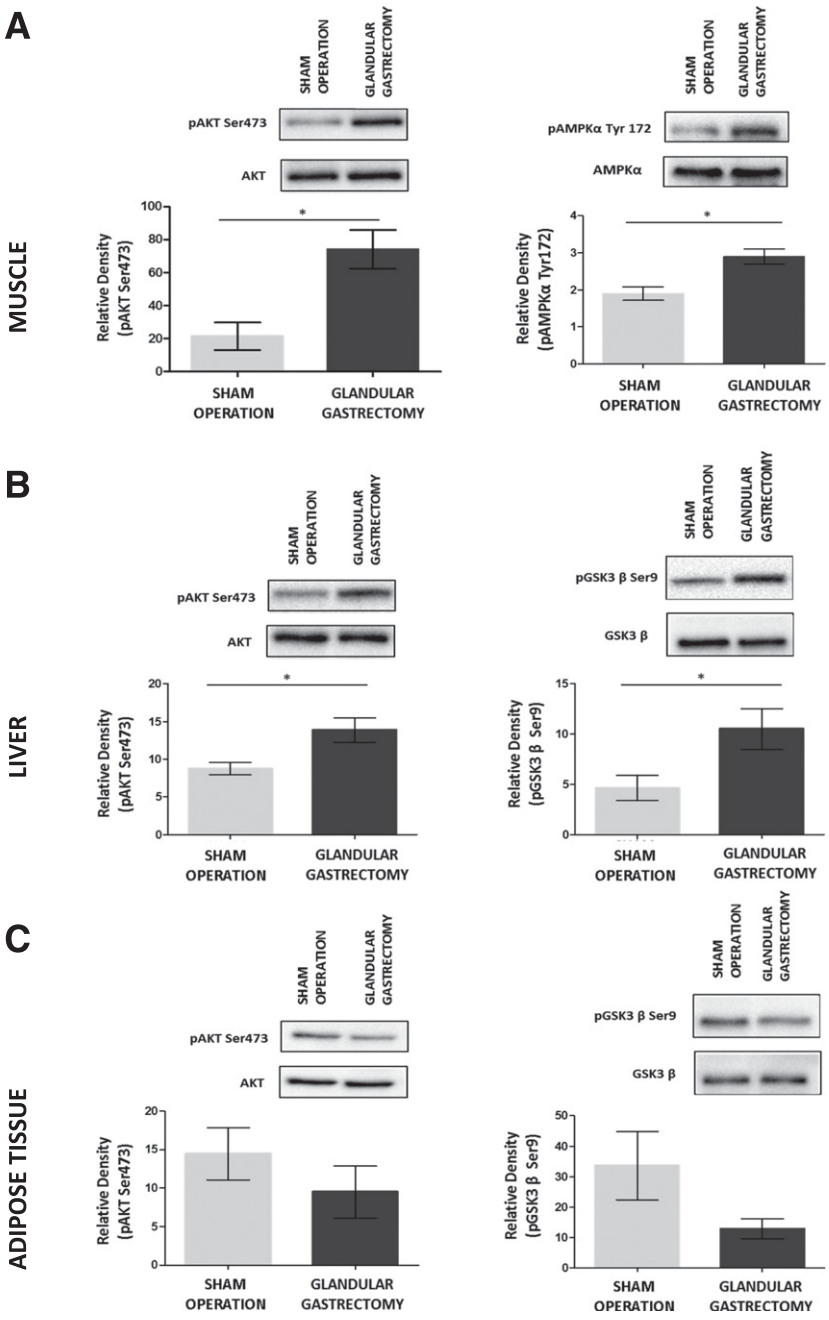

Figure 3—Densitometric analyses of phosphorylated/total protein in 15 muscle samples of SO and GG rats obtained at kill. Data are mean ± SEM. Representative blot of a single rat (SO and GG) is shown. *A*: Level of Akt phosphorylation (Ser473) in muscle biopsy specimens from SO and GG rats (left) showed a low level of phosphorylation of Ser473 in SO rats and a significant increase of phosphorylation after GG (21.5 ± 8.2 vs. 74.03 ± 11.8%, $P = 0.006$); GG rats exhibited increased phosphorylation of AMPKα (Tyr172) compared with SO rats (1.9 ± 0.18 vs. 2.9 ± 0.2%, $P = 0.007$) (right). *B*: Level of Akt phosphorylation (Ser473) in liver biopsy specimens of SO and GG rats (left) showed a low level of phosphorylation of Ser473 in SO rats and a significant increase of phosphorylation after GG (8.7 ± 0.8 vs. 13.9 ± 1.7%, $P = 0.03$); level of GSK3β phosphorylation (Ser9) in liver biopsy specimens of SO and GG rats (right) showed a low level of phosphorylation of Ser9 in SO rats and a significant increase of phosphorylation after GG (4.6 ± 1.3 vs. 10.5 ± 2%, $P = 0.03$). GSK3α was not detected. *C*: Level of Akt phosphorylation (Ser473) in adipose tissue biopsy specimens of SO and GG rats (left) showed no significant difference in phosphorylation after GG (16.1 ± 3.4 vs. 9.4 ± 3.4%); level of GSK3β phosphorylation (Ser9) in adipose tissue biopsy specimens of SO and GG rats (right) showed no significant difference of phosphorylation after GG (38.7 ± 11.2 vs. 12.6 ± 3.5%). GSK3α was not detected. *$P < 0.03$.

reduction of ectopic fat deposition and redistribution of body fat, *2*) improvement of insulin resistance, *3*) changes in the gut microbiota profile with an increase primarily of Lactobacilli, an but also increase of microbial diversity, and an alteration of BA pool size, and *4*) a decrease in low-grade inflammation state as shown by reduced concentrations of circulating LPS as well as cellular infiltrates and fibrosis in adipose tissue. Compared with SO, GG did

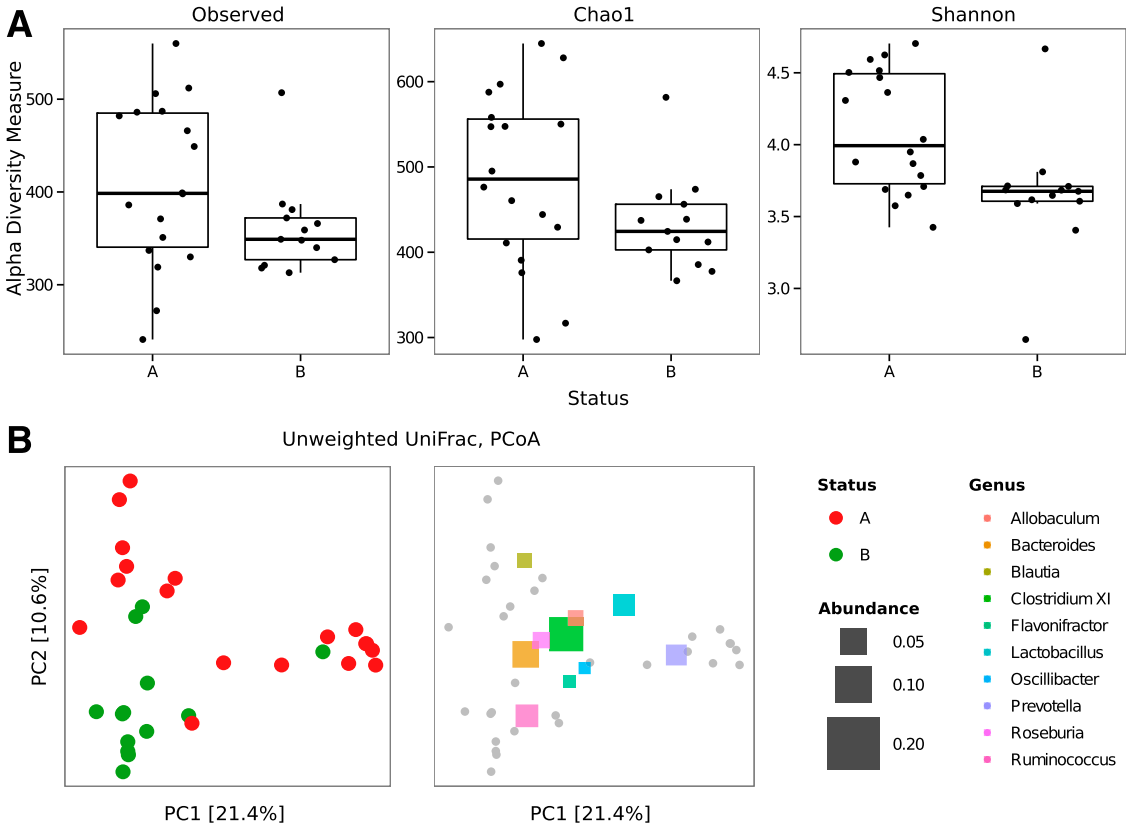

Figure 4—*A*: α-Diversity from genus to phylum level for GG (A) and SO rats (B) measured using number of observed taxa, Chao1 index, and Shannon entropy. The horizontal line in each box indicates the median, and the box extends to the 25th and 75th percentiles. *B*: Principal components analysis (PCoA) of between-sample distances (β-diversity) computed by using the unweighted UniFrac distance. The right panel shows the same PCoA plot with the 10 most abundant genera (showing the highest average relative abundance across all samples) overlaid as colored squares with a size proportional to their mean relative abundance. Genus coordinates were calculated as the weighted average across sample coordinates. PC, principal component.

not induce significant body weight loss or reduced food intake after the first 3 weeks following the operations. However, we did not measure the impact of GG on intestinal transit or whether it altered meal frequency or size.

The weight loss observed in GG and SO rats during the first 2 weeks after surgery agrees with that reported in the literature for rodents fed an HFD after conventional SG or SO (12,13), with ~18% weight reduction from baseline. However, although the weight gain curve after conventional SG remains significantly lower than in SO rats (12,13), the current series showed no difference in weight gain between GG and SO animals over time. This suggests that the rapid fall of circulating ghrelin levels following GG acutely reduces appetite, but because the aglandular stomach remains intact (the gastric section responsible for food storage and digestion in rat), this may permit normal food intake comparable to that of SO rats. The model was not designed to measure the early dynamic effects of GG but rather to shed light on the steady effects of this operation. In fact, the GG rats ate ~50% fewer calories for a full 2 weeks following the operation, and this might have resulted in loss of fat and lean mass and improvements in glycemic control. We do not know whether this weight loss period might have influenced the findings observed at the end of the study, although a further 8 weeks during which GG animals rapidly gained weight should be a long enough period to minimize the effect of these 2 weeks of hypocaloric intake. Given that days in rats translates into months for humans, we cannot extrapolate the results to humans, where some types of bariatric/metabolic operations improve insulin action just days after surgery, independently of weight loss. Further monitoring of insulin sensitivity during the weight loss period as well as in the regaining phase would be useful and would provide additional mechanistic evidence.

The HFD determined insulin resistance and fat deposition in both liver and skeletal muscle tissue in SO rats, whereas GG prevented these features and determined redistribution of the adiposity pattern characterized by decreased visceral fat and by proportionally increased subcutaneous fat. Fat redistribution may have played an important role in modulating insulin resistance. Visceral fat weight was directly associated with HOMA-IR. Of note, partial surgical removal of intraabdominal fat prevents the onset of age-dependent insulin resistance and significantly delays the onset of glucose intolerance

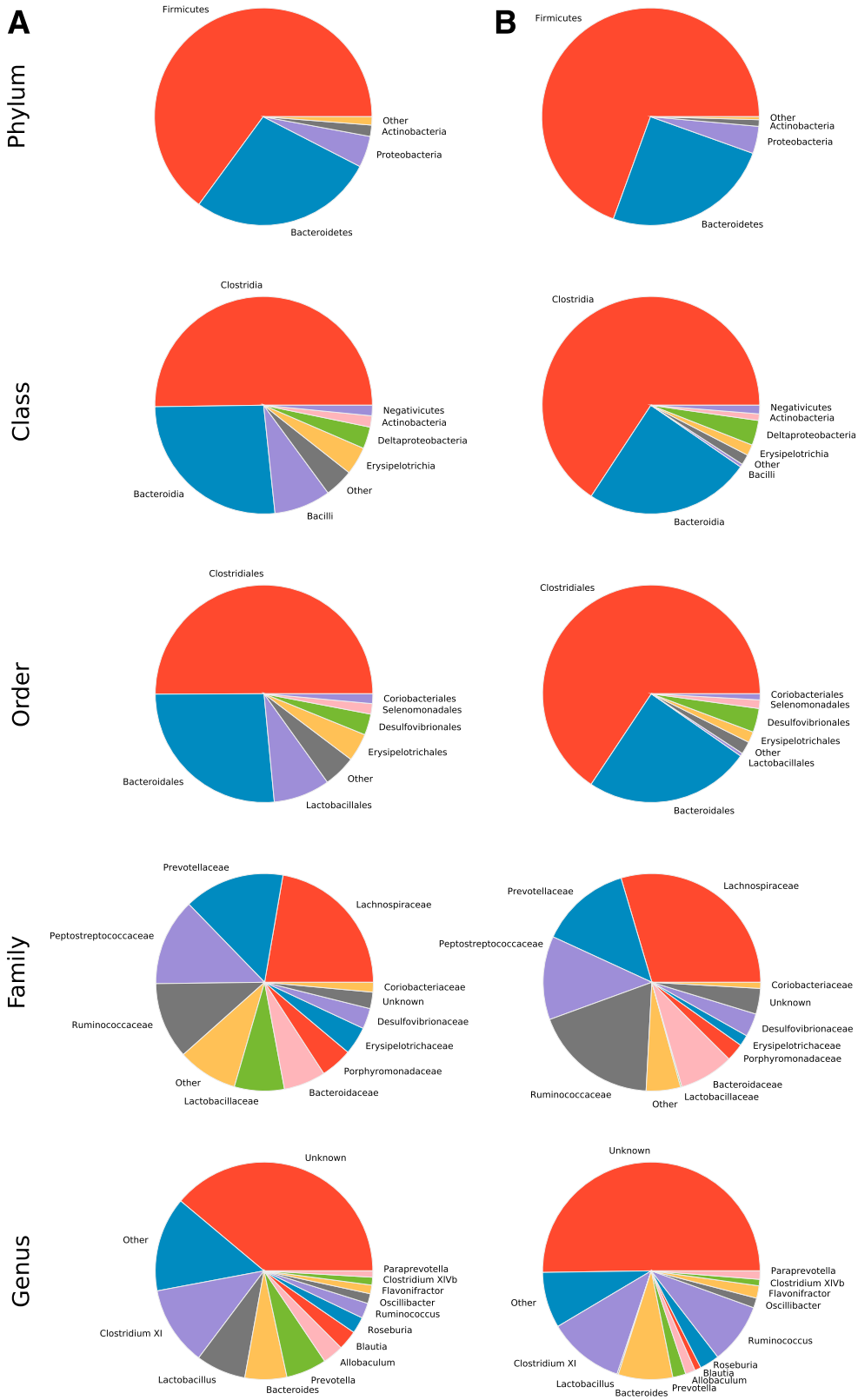

Figure 5—Differences in relative abundance of taxa from phylum to genus level for GG (*A*) and SO (*B*) animals. Taxa with relative abundance <1% are merged into the other label.

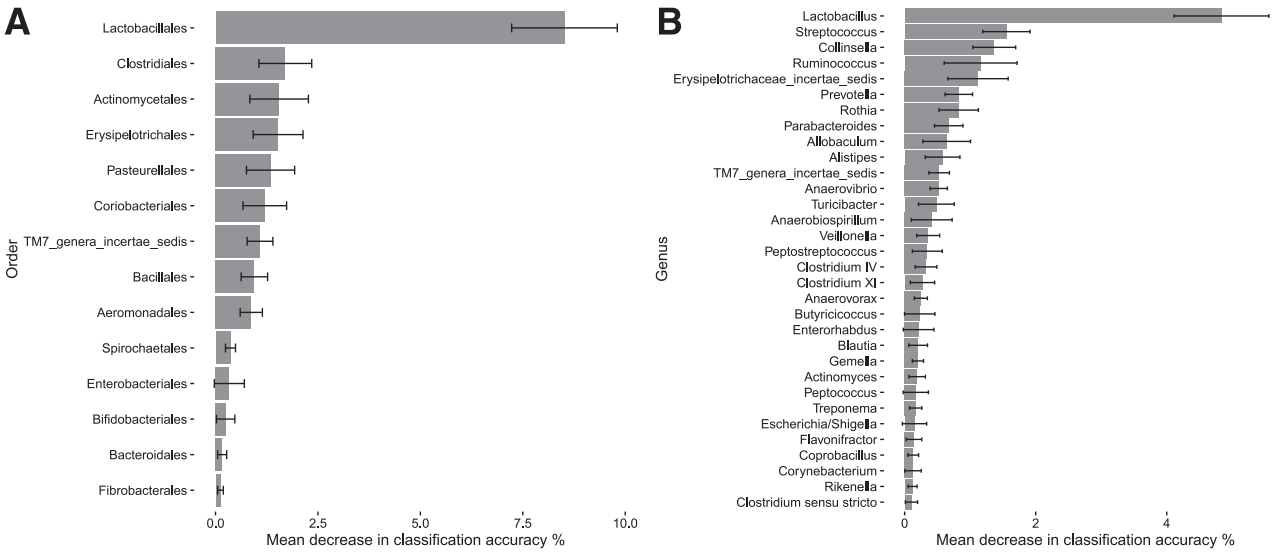

Figure 6—Top-ranked orders (*A*) and genera (*B*) identified by random forest analysis according to their ability to discriminate the microbiota of GG and SO rats in decreasing order of discriminatory importance (mean decrease in classification accuracy >0.1%). Importance was determined on the basis of the expected mean decrease in classification accuracy when the feature was ignored. Error bars indicate SD.

and diabetes in rodent models of obesity and diabetes (14). GG used in the current series provides a model of metabolically healthy obesity. In humans, metabolically healthy but obese individuals have significantly lower levels of visceral fat and are resistant to the metabolic and cardiovascular risks that derive from obesity (15). Furthermore, metabolically healthy but obese individuals appear to have higher microbial diversity both in species and gene richness compared with other obese individuals (16).

It has been shown that BA (ursodeoxycholic acid) ingestion decreases age-related adiposity and inflammation in mice (17). Circulating levels of BAs and composition are regulated by gut microbiota (18,19), and we found that the plasma levels of total BAs were significantly and inversely correlated with HOMA-IR in a multiple regression analysis. In addition, accumulation of glycogen was observed only in the liver of SO rats. A net liver glycogen accumulation is described in ~80% of patients with diabetes (20) as well as in obese patients (21) and has been suggested to be linked to enhanced gluconeogenesis. Therefore, GG modifies adipose tissue distribution by preventing ectopic fat deposition and reduces liver glycogen accumulation possibly as a consequence of the drastic reduction of ghrelin secretion and of the less pronounced increase in GLP-1 levels, which have been linked to changes in the gut microbiome and circulating BAs (22–24).

GG also improved insulin signaling. We found a significantly higher phosphorylation of Akt in both liver and skeletal muscle of GG compared with SO rats. Once phosphorylated on both Thr308 and Ser473, Akt is fully activated and phosphorylates its downstream effector GSK3β (25), which was significantly more phosphorylated in GG than in SO rats. GSK3β phosphorylation on Ser9 or Ser21, depending on tissue-specific isoform expression, decreases its active site availability. Because GSK3 is a protein kinase that phosphorylates and inactivates glycogen synthesis, the rate-limiting enzyme in glycogen formation (26), its inactivation stimulates glycogen production. Therefore, although we did not measure it directly, the accumulation of glycogen in SO rat tissues is a likely consequence of impaired glycogen breakdown. Cellular glycogen results from the balance between synthesis and glycogenolysis. Both hyperglycemia and hyperinsulinemia are potent inhibitors of glycogenolysis (27,28); thus, HFD induction of insulin resistance may reduce glycogenolysis with subsequent glycogen accumulation. Furthermore, in hyperglycemic conditions, glucose passively enters the hepatocytes by insulin-independent GLUT2 and is rapidly phosphorylated, with inhibition of its release from hepatocytes (29).

Fully phosphorylated Akt, as observed in GG rats, suppresses hepatic glucose production by decreasing the expression of gluconeogenic enzymes by phosphorylation and nuclear exclusion of the forkhead box protein FOXO1 and its progluconeogenic targets (30). These functional cellular findings may explain why HOMA-IR, an index of hepatic insulin resistance, and the AUC glucose-to-insulin ratio, indicative of peripheral insulin resistance, were markedly reduced only in GG rats. In fact, HFD impairs the insulin signaling determining hepatic and peripheral insulin resistance by reducing Akt and GSK phosphorylation and function. However, glycemia did not return to baseline values in both GG and SO rats after the OGTT (Fig. 1), suggesting that the glucose clearance from the circulation to the metabolic compartment is not fully normalized by GG.

For the mechanism of action of GG on the normalization of insulin resistance, three possible factors, namely the

abolition of ghrelin secretion, increased circulating GLP-1, and elevation of BAs, might have played a significant role. According to our findings (i.e., GG rats did not appreciably lose weight), *ghrelin*$^{-/-}$ mice fed an HFD do not show appetite reduction or weight loss (31). *Ghrelin*$^{-/-}$ mice show improved glucose tolerance and increased insulin sensitivity (32). Of note, also in ghrelin receptor knockout mice (i.e., mice producing ghrelin that cannot bind to its receptor), peripheral insulin sensitivity is greatly increased, whereas hepatic glucose production is reduced (33). Thus, the most important role of ghrelin appears to be that of regulating insulin sensitivity and glucose homeostasis.

We cannot exclude, however, that the marked improvement of insulin sensitivity observed in this series is partially explained by the increase of GLP-1 secretion or by changes in gut microbiota profile and resultant changes in BA pool size. The lack of DPP-4, the enzyme that degrades GLP-1, has been demonstrated to improve HOMA-IR and the OGTT AUC in genetically DPP-4–deficient rats (F344/DuCrj) fed an HFD compared with F344/Crj control rats (34). Microbially produced short-chain fatty acids, BAs, and certain probiotic strains (e.g., *Lactobacillus reuteri* SD5865) stimulate glucose-induced GLP-1 release (22,35,36).

The literature on the gut microbiota profiles in obesity and after metabolic surgery are consistent in showing dramatic effects on microbial make-up but less so in terms of which organisms or microbial-related metabolic activities are affected. The first studies in *ob/ob* mice demonstrated that the Firmicutes were more represented, whereas the Bacteroidetes were correspondingly reduced (37), and this was considered an imprinting of obesity. However, successively using an *ob/ob* mouse model fed either a low-fat diet or an HFD and comparing it with wild-type mice, Murphy et al. (38) demonstrated that an increased Firmicutes/Bacteroidetes ratio was the result of the HFD rather than genetic obesity. Accordingly, Turnbaugh et al. (39) found that in diet-induced obese mice, the difference in Firmicutes/Bacteroidetes ratio was mainly related to the increase in a single class of bacteria, the Mollicutes, which belongs to the Firmicutes phylum. After gastric bypass in a rat model, Li et al. (40) showed a simultaneous reduction of both Firmicutes (4.5-fold) and Bacteroidetes (twofold) compared with SO rats but a significant increase of Proteobacteria (52-fold), which are a phylum of gram-negative bacteria. In the current study, we found no significant changes in the Firmicutes/Bacteroidetes ratio between GG and SO rats fed an HFD; rather, we found dramatic shifts in relative abundance within the Firmicutes, with increased relative abundance of *Lactobacillus* and reduced abundance of *Ruminococcus* characterizing improved metabolic health in the GG animals. Indeed, our random forest analysis showed Lactobacilli to be the main bacteria taxon distinguishing GG from SO animals.

GG was associated with reduced endotoxemia as shown by the lower circulating levels of LPS compared with SO rats. Luche et al. (41) demonstrated that metabolic endotoxemia increases macrophage number in mouse adipose tissue in a CD14-mediated manner. Accordingly, the visceral adipose tissue of SO rats showed an increased cellular infiltration and fibrosis not observed after GG rats.

We acknowledge some limitations of this study. The model is markedly different from the human model, where improvements in glycemic control are generally observed during the period of weight loss. However, we note that after biliopancreatic diversion, patients become extremely insulin sensitive, even though they have lost negligible amounts of weight (8) or pass from super obesity to morbid obesity (42). In addition, the gastric anatomy of the rat is different from that of humans, where the glands containing endocrine cells are distributed throughout the entire gastric surface, thus preventing replication of this operation in patients. Finally, we did not test the mechanistic aspects of the observed metabolic changes.

In conclusion, the GG we devised shows a role of the stomach in glycemia even though the rats essentially remained obese. It lowered insulin resistance—through the improvement of both insulin-mediated hepatic and peripheral insulin sensitivity, with an increase of Akt and GSK3 phosphorylation and insulin-independent glucose disposal as demonstrated by the increased muscular phosphorylation of AMPK—and reduced ectopic fat deposition and hepatic glycogen overaccumulation. These findings are associated with body adipose tissue redistribution; net reduction of intraabdominal fat; dramatic reduction of circulating ghrelin levels; increased GLP-1 plasma concentration; and remodeling of the gut microbiome with an increased taxonomic richness, increased relative abundance of Lactobacilli, and increased circulating BA pool. Collectively, these data suggest that in the rat, the secreting portion of the stomach plays a central role in improvement of the metabolic syndrome.

Acknowledgments. The authors thank Anna Caprodossi (Department of Internal Medicine, Catholic University, Rome, Italy) for excellent technical support.
Funding. This study was partially supported by the grant 70201398-LINEA D.1 2015 from Catholic University. A.L.B. was supported by a grant from the German Diabetes Association.
Duality of Interest. No potential conflicts of interest relevant to this article were reported.
Author Contributions. N.B. contributed to the study design, data research, operations, and writing of the manuscript. E.S. contributed to the data research and operations. L.C.-G. and G.C. contributed to the data research, operations, and discussion. D.A. and C.D. contributed to the experiments on gut microbiota and statistical analysis. F.F. and K.T. contributed to the experiments on gut microbiota, statistical analysis, and writing of the manuscript. G.A., F.L.N., and A.S. contributed to the Western blots. V.K.-L. contributed to the writing of the manuscript. A.L.B., S.B., and M.M. contributed to the discussion. G.M. contributed to the study design and writing of the manuscript. G.M. is the guarantor of this work and, as such, had full access to all the data in the study and takes responsibility for the integrity of the data and the accuracy of the data analysis.

References

1. Wadden TA, Butryn ML, Byrne KJ. Efficacy of lifestyle modification for long-term weight control. Obes Res 2004;12(Suppl.):151S–162S
2. Mingrone G, Panunzi S, De Gaetano A, et al. Bariatric surgery versus conventional medical therapy for type 2 diabetes. N Engl J Med 2012;366:1577–1585

3. Schauer PR, Kashyap SR, Wolski K, et al. Bariatric surgery versus intensive medical therapy in obese patients with diabetes. N Engl J Med 2012;366:1567–1576
4. Schauer PR, Bhatt DL, Kirwan JP, et al.; STAMPEDE Investigators. Bariatric surgery versus intensive medical therapy for diabetes—3-year outcomes. N Engl J Med 2014;370:2002–2013
5. Mingrone G, Panunzi S, De Gaetano A, et al. Bariatric-metabolic surgery versus conventional medical treatment in obese patients with type 2 diabetes: 5 year follow-up of an open-label, single-centre, randomised controlled trial. Lancet 2015;386:964–973
6. DeFronzo RA, Tripathy D. Skeletal muscle insulin resistance is the primary defect in type 2 diabetes. Diabetes Care 2009;32(Suppl. 2):S157–S163
7. Pories WJ, Swanson MS, MacDonald KG, et al. Who would have thought it? An operation proves to be the most effective therapy for adult-onset diabetes mellitus. Ann Surg 1995;222:339–350; discussion 350–352
8. Guidone C, Manco M, Valera-Mora E, et al. Mechanisms of recovery from type 2 diabetes after malabsorptive bariatric surgery. Diabetes 2006;55:2025–2031
9. Basso N, Capoccia D, Rizzello M, et al. First-phase insulin secretion, insulin sensitivity, ghrelin, GLP-1, and PYY changes 72 h after sleeve gastrectomy in obese diabetic patients: the gastric hypothesis. Surg Endosc 2011;25:3540–3550
10. Robert A. Proposed terminology for the anatomy of the rat stomach. Gastroenterology 1971;60:344–345
11. Matthews DR, Hosker JP, Rudenski AS, Naylor BA, Treacher DF, Turner RC. Homeostasis model assessment: insulin resistance and beta-cell function from fasting plasma glucose and insulin concentrations in man. Diabetologia 1985;28:412–419
12. Rodríguez A, Becerril S, Valentí V, et al. Short-term effects of sleeve gastrectomy and caloric restriction on blood pressure in diet-induced obese rats. Obes Surg 2012;22:1481–1490
13. Valentí V, Martín M, Ramírez B, et al. Sleeve gastrectomy induces weight loss in diet-induced obese rats even if high-fat feeding is continued. Obes Surg 2011;21:1438–1443
14. Gabriely I, Ma XH, Yang XM, et al. Removal of visceral fat prevents insulin resistance and glucose intolerance of aging: an adipokine-mediated process? Diabetes 2002;51:2951–2958
15. Hwang YC, Hayashi T, Fujimoto WY, et al. Visceral abdominal fat accumulation predicts the conversion of metabolically healthy obese subjects to an unhealthy phenotype. Int J Obes 2015;39:1365–1370
16. Cotillard A, Kennedy SP, Kong LC, et al.; ANR MicroObes consortium. Dietary intervention impact on gut microbial gene richness. Nature 2013;500:585–588
17. Oh AR, Bae JS, Lee J, et al. Ursodeoxycholic acid decreases age-related adiposity and inflammation in mice. BMB Rep 2016;49:105–110
18. Midtvedt T. Microbial bile acid transformation. Am J Clin Nutr 1974;27:1341–1347
19. Ridlon JM, Kang DJ, Hylemon PB. Bile salt biotransformations by human intestinal bacteria. J Lipid Res 2006;47:241–259
20. Ferrannini E, Lanfranchi A, Rohner-Jeanrenaud F, Manfredini G, Van de Werve G. Influence of long-term diabetes on liver glycogen metabolism in the rat. Metabolism 1990;39:1082–1088
21. Creutzfeldt W, Frerichs H, Sickinger K. Liver diseases and diabetes mellitus. Prog Liver Dis 1970;3:371–407
22. Simon MC, Strassburger K, Nowotny B, et al. Intake of *Lactobacillus reuteri* improves incretin and insulin secretion in glucose-tolerant humans: a proof of concept. Diabetes Care 2015;38:1827–1834
23. Okubo H, Nakatsu Y, Sakoda H, et al. Mosapride citrate improves non-alcoholic steatohepatitis with increased fecal lactic acid bacteria and plasma glucagon-like peptide-1 level in a rodent model. Am J Physiol Gastrointest Liver Physiol 2015;308:G151–G158
24. Murakami M, Une N, Nishizawa M, Suzuki S, Ito H, Horiuchi T. Incretin secretion stimulated by ursodeoxycholic acid in healthy subjects. Springerplus 2013;2:20
25. Ishiki M, Klip A. Minireview: recent developments in the regulation of glucose transporter-4 traffic: new signals, locations, and partners. Endocrinology 2005;146:5071–5078
26. Hemmings BA, Aitken A, Cohen P, Rymond M, Hofmann F. Phosphorylation of the type-II regulatory subunit of cyclic-AMP-dependent protein kinase by glycogen synthase kinase 3 and glycogen synthase kinase 5. Eur J Biochem 1982;127:473–481
27. Adkins A, Basu R, Persson M, et al. Higher insulin concentrations are required to suppress gluconeogenesis than glycogenolysis in nondiabetic humans. Diabetes 2003;52:2213–2220
28. Petersen KF, Laurent D, Rothman DL, Cline GW, Shulman GI. Mechanism by which glucose and insulin inhibit net hepatic glycogenolysis in humans. J Clin Invest 1998;101:1203–1209
29. Chatila R, West AB. Hepatomegaly and abnormal liver tests due to glycogenosis in adults with diabetes. Medicine (Baltimore) 1996;75:327–333
30. Matsumoto M, Pocai A, Rossetti L, Depinho RA, Accili D. Impaired regulation of hepatic glucose production in mice lacking the forkhead transcription factor Foxo1 in liver. Cell Metab 2007;6:208–216
31. Sun Y, Butte NF, Garcia JM, Smith RG. Characterization of adult ghrelin and ghrelin receptor knockout mice under positive and negative energy balance. Endocrinology 2008;149:843–850
32. Sun Y, Asnicar M, Saha PK, Chan L, Smith RG. Ablation of ghrelin improves the diabetic but not obese phenotype of ob/ob mice. Cell Metab 2006;3:379–386
33. Qi Y, Longo KA, Giuliana DJ, et al. Characterization of the insulin sensitivity of ghrelin receptor KO mice using glycemic clamps. BMC Physiol 2011;11:1
34. Yasuda N, Nagakura T, Yamazaki K, Inoue T, Tanaka I. Improvement of high fat-diet-induced insulin resistance in dipeptidyl peptidase IV-deficient Fischer rats. Life Sci 2002;71:227–238
35. Psichas A, Sleeth ML, Murphy KG, et al. The short chain fatty acid propionate stimulates GLP-1 and PYY secretion via free fatty acid receptor 2 in rodents. Int J Obes 2015;39:424–429
36. Vettorazzi JF, Ribeiro RA, Borck PC, et al. The bile acid TUDCA increases glucose-induced insulin secretion via the cAMP/PKA pathway in pancreatic beta cells. Metabolism 2016;65:54–63
37. Ley RE, Bäckhed F, Turnbaugh P, Lozupone CA, Knight RD, Gordon JI. Obesity alters gut microbial ecology. Proc Natl Acad Sci U S A 2005;102:11070–11075
38. Murphy EF, Cotter PD, Healy S, et al. Composition and energy harvesting capacity of the gut microbiota: relationship to diet, obesity and time in mouse models. Gut 2010;59:1635–1642
39. Turnbaugh PJ, Bäckhed F, Fulton L, Gordon JI. Diet-induced obesity is linked to marked but reversible alterations in the mouse distal gut microbiome. Cell Host Microbe 2008;3:213–223
40. Li JV, Ashrafian H, Bueter M, et al. Metabolic surgery profoundly influences gut microbial-host metabolic cross-talk. Gut 2011;60:1214–1223
41. Luche E, Cousin B, Garidou L, et al. Metabolic endotoxemia directly increases the proliferation of adipocyte precursors at the onset of metabolic diseases through a CD14-dependent mechanism. Mol Metab 2013;2:281–291
42. Mari A, Manco M, Guidone C, et al. Restoration of normal glucose tolerance in severely obese patients after bilio-pancreatic diversion: role of insulin sensitivity and beta cell function. Diabetologia 2006;49:2136–2143